

Optical spectroscopy of X-ray sources in the old open cluster M 67 [★]

Maureen van den Berg¹, Frank Verbunt¹, and Robert D. Mathieu²

¹ Astronomical Institute, P.O.Box 80000, 3508 TA Utrecht, The Netherlands

² Department of Astronomy, University of Wisconsin, Madison, WI 53706, U.S.A.

Received date / Accepted date

Abstract. We have obtained optical spectra of seven stars in the old galactic cluster M67 that are unusual sources of X-rays, and investigate whether the X-ray emission is due to magnetic activity or to mass transfer. The two binaries below the giant branch S1063 and S1113, the giant with the white dwarf companion S1040 and the eccentric binary on the subgiant branch S1242 show magnetic activity in the form of Ca II H&K emission and H α emission, suggesting that their X-rays are coronal. The reason for the enhanced activity level in S1040 is not clear. The two wide, eccentric binaries S1072 and S1237 and the blue straggler S1082 do not show evidence for Ca II H&K emission. A second spectral component is found in the spectrum of S1082, most clearly in the variable H α absorption profile. We interpret this as a signature of the proposed hot subluminescent companion.

Key words: Stars: activity – binaries: general – open clusters and associations: individual: M 67 – X-rays: stars

Table 1. Stars of M67 discussed in this paper. Visual magnitude and colour (from Montgomery et al. 1993), spectral type (from Allen & Strom 1995, and Zhilinskii & Frolov 1994), orbital period and eccentricity (from Mathieu et al. 1990, Latham et al. 1992 and – for S1113 – Mathieu et al. 1999, in preparation), and X-ray count rate in PSPC channels 41–240, corresponding to 0.4–2.4 keV (from Belloni et al. 1998).

| ID | <i>V</i> | <i>B-V</i> | sp.type | <i>P</i> _b (d) | <i>e</i> | ctrate (s ⁻¹) |
|--------|----------|------------|----------|------------------------------|-----------|------------------------------|
| S 1040 | 11.52 | 0.87 | G4III | 42.83 | 0.027(28) | 0.0050(6) |
| S 1063 | 13.79 | 1.05 | G8IV | 18.39 | 0.217(14) | 0.0047(6) |
| S 1072 | 11.32 | 0.61 | G3III–IV | 1495. | 0.32(7) | 0.0013(3) |
| S 1082 | 11.25 | 0.42 | F5IV | | | 0.0046(6) |
| S 1113 | 13.77 | 1.01 | | 2.823 | 0.031(14) | 0.0047(6) |
| S 1237 | 10.78 | 0.94 | G8III | 697.8 | 0.105(15) | 0.0010(3) |
| S 1242 | 12.72 | 0.68 | | 31.78 | 0.664(18) | 0.0007(2) |

1. Introduction

Two observations of M67 with the ROSAT PSPC resulted in the detection of X-ray emission from 25 members of this old open cluster (Belloni et al. 1993, 1998). The X-ray emission of many of these sources is readily understood. For example, the X-ray emission originates in deep, hot atmospheric layers in a hot white dwarf; is due to mass transfer in a cataclysmic variable; and is caused by magnetic activity in two contact binaries and several RS CVn-type binaries. However, Belloni et al. (1998) point out several X-ray sources in M67 for which the X-ray emission is unexplained. All but one of these objects are located away from the isochrone formed by the main sequence and the (sub)giant branch of M67 (Fig. 1).

Send offprint requests to: Maureen van den Berg

[★] Based on observations made with the William Herschel Telescope operated on the island of La Palma by the Isaac Newton Group in the Spanish Observatorio del Roque de los Muchachos of the Instituto de Astrofísica de Canarias

Correspondence to: m.c.vandenberg@astro.uu.nl

In this paper we investigate the nature of the X-ray emission of these stars through low- and high-resolution optical spectra. In particular, we investigate whether the emission could be coronal as a consequence of magnetic activity, by looking for emission cores in the Ca II H&K lines. Tidal interaction in a close binary orbit is thought to enhance magnetic activity at the stellar surface by spinning up the stars in the binary. Therefore, we also derive projected rotational velocities with the crosscorrelation method. Finally, we study the H α profile as a possible indicator of activity or mass transfer.

The observations and the data reduction are described in Sect. 2, and the analysis of the spectra in Sect. 3. Comparison with chromospherically active binaries is made in Sect. 4. A discussion of our results is given in Sect. 5. In the remainder of the introduction we give brief sketches of the stars studied in this paper; details on many of them are given by Mathieu et al. (1990). The stars are indicated with their number in Sanders (1977), and are listed in Table 1.

S 1063 and S 1113 are two binaries located below the subgiant branch in the colour-magnitude diagram of M 67. Their orbital periods, 18.4 and 2.82 days respectively, are too long for them to be contact binaries; also they are too far above the main sequence to be binaries of main-sequence stars. In principle, a (sub)giant can become underluminous when it transfers mass to its companion, as energy is taken from the stellar luminosity to restore hydrostatic equilibrium (e.g. Kippenhahn & Weigert 1967). However, mass transfer through Roche lobe overflow very rapidly leads to circularization of the binary orbit, whereas S 1063 has an eccentricity $e = 0.217$. The orbit of S 1113 is circular, so mass transfer could be occurring in that system. For the moment, the nature of these binaries is not understood. In both, Pasquini & Belloni (1998) observed emission cores in the Ca II H&K lines. S 1063 is reported to be photometrically variable with ~ 0.10 mag (Rajamohan et al. 1988; Kaluzny & Raczynska 1991), but no period is found. For S 1113, photometric variability with a period of 0.313 days and a total amplitude of 0.6 mag was claimed by Kurochkin (1960), but this has not been confirmed by Kaluzny & Raczynska (1991), who find variability with only 0.05 mag. S 1063 is the only M 67 star in our sample that shows significantly variable X-ray emission (between 0.0081 and 0.0047 cts s $^{-1}$; Belloni et al. 1998).

S 1072 and S 1237 are binaries with orbital periods of 1495 and 698 days, and with eccentricities $e = 0.32$ and 0.105, respectively. The colour and magnitude of S 1072 cannot be explained with the pairing of a giant and a blue straggler, since this is not compatible with its *ubvy* photometry (Nissen et al. 1987; Mathieu & Latham 1986), nor with superposition of three subgiants, since this is excluded by the radial velocity correlations (Mathieu et al. 1990). The absence of the 6708 Å lithium feature in the spectrum of S 1072 indicates that the surface material has undergone mixing (Hobbs & Mathieu 1991; Pritchett & Glaspey 1991). S 1237 could be a binary of a giant and a star at the top of the evolved main sequence (Janes & Smith 1984); high-resolution spectroscopy should be able to detect the main-sequence star in that case (Mathieu et al. 1990). The wide orbits and significant eccentricities appear to exclude both mass transfer and tidal interaction as explanations for the X-ray emission.

S 1242 has the largest eccentricity of the binaries in our sample, at $e = 0.66$ in an orbit of 31.8 days. Its position on the subgiant branch is explained if a subgiant of $1.25 M_{\odot}$ has a secondary with $V > 15$ (Mathieu et al. 1990). Ca II K line emission is reported by Pasquini & Belloni (1998). Photometric variability with a period of 4.88 days and amplitude of 0.0025 mag has been found by Gilliland et al. (1991). We note that this photometric period corresponds to corotation with the orbit at periastron, which suggests that the X-ray emission may be due to tidal interaction taking place at periastron. The binary would then be an interesting example of a system in transition from an eccentric to a circular orbit. Indeed, according to the diag-

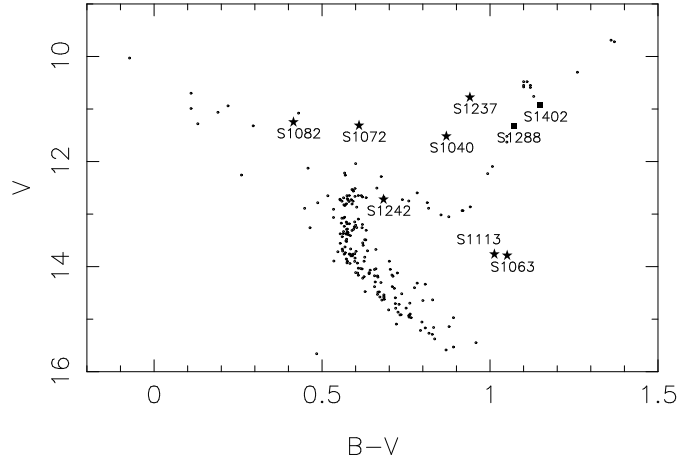


Fig. 1. Colour-magnitude diagram of M 67. Colours and magnitudes are from Montgomery et al. (1993). Only stars with membership probability > 0.8 (based on their proper motion, Sanders 1977) were selected. Stars indicate the observed X-ray binaries; squares two member giants observed for comparison.

nostic diagram of Verbunt & Phinney (1995) a giant of $1.25 M_{\odot}$ with a current radius of $\simeq 2.3 R_{\odot}$ (as derived from the location of S 1242 in the colour-magnitude diagram) cannot have circularized an orbit of 31.8 days.

S 1040 is a binary consisting of a giant and a white dwarf. The progenitor of the white dwarf circularized the orbit during a phase of mass transfer (Verbunt & Phinney 1995); as a result the mass of the white dwarf is very low (Landsman et al. 1997). The white dwarf is probably too cool, at 16 160 K, to be the X-ray emitter. Indications for magnetic activity are Ca II H&K (Pasquini & Belloni 1998) and Mg II ($\lambda\lambda$ 2800 Å, Landsman et al. 1997) emission lines. If the X-rays are due to coronal emission of the giant, this must be the consequence of the past evolution of the binary, since the giant is too small for significant tidal interaction to be taking place in the current orbit.

S 1082 is a blue straggler. Photometric variability of 0.08 mag within a few hours was observed by Simoda (1991). Goranskii et al. (1992) found eclipses with a total amplitude of 0.12 mag and a binary period of 1.07 days; however, the radial velocities of the star do not show this period, and vary by about 2 km s $^{-1}$, far too little for a 1 day eclipsing binary (Mathieu et al. 1986). Landsman et al. (1998) detect a significant excess at 1520 Å with the Ultraviolet Imaging Telescope, and ascribe this to a hot, subluminous secondary. Such a secondary was suggested already by Mathys (1991) on the basis of a broad component in the Na I D and O I absorption lines.

2. Observations and data reduction

Optical spectra were obtained on February 28/29, 1996 with the 4.2m William Herschel Telescope on La Palma, under good weather conditions (seeing $< 1''$ until 4 h 30

Table 2. Log of the observations. For each target we give the UT at start of the exposures and the exposure time for the ISIS and UES blue and red spectra. All observations were obtained on 28/29 February 1996, except the blue UES exposures of S 1113 which were taken on 7/8 April 1998 (indicated with * in the table).

| ID | ISIS | | UES blue | | UES red | |
|--------------------|-------|-------------------------|----------|-------------------------|---------|-------------------------|
| | UT | t_{exp} (s) | UT | t_{exp} (s) | UT | t_{exp} (s) |
| TARGETS | | | | | | |
| S 1040 | 02:43 | 60 | 22:03 | 600 | 00:46 | 300 |
| S 1063 | 02:30 | 180 | 20:51 | 1200 | 00:11 | 1200 |
| | | | 21:15 | 1200 | 00:33 | 600 |
| | | | 21:37 | 1200 | | |
| S 1072 | 02:49 | 60 | 22:24 | 360 | 01:01 | 240 |
| S 1082 | 02:39 | 60 | 20:39 | 300 | 00:01 | 360 |
| | | | 23:24 | 600 | 01:41 | 360 |
| | | | | | 04:11 | 360 |
| S 1113 | 03:01 | 180 | 22:37* | 900 | 03:36 | 1200 |
| | | | 22:58* | 900 | 03:58 | 600 |
| S 1237 | 02:46 | 60 | 22:16 | 300 | 00:54 | 180 |
| S 1242 | 02:55 | 120 | 22:33 | 1500 | 01:08 | 900 |
| COMPARISON GIANTS | | | | | | |
| S 1288 | 02:58 | 60 | 23:12 | 600 | 01:33 | 300 |
| S 1402 | 02:52 | 60 | 23:01 | 450 | 01:26 | 240 |
| FLUX STANDARD | | | | | | |
| HZ 44 | 02:21 | 80 | 23:42 | 600 | 01:57 | 600 |
| | 03:13 | 80 | | | | |
| | 04:43 | 480 | | | | |
| VELOCITY STANDARDS | | | | | | |
| HD 132737 | | | 06:04 | 90 | 05:13 | 45 |
| HD 136202 | | | 05:55 | 100 | 05:42 | 50 |
| HD 171232 | | | | | 05:34 | 45 |

UT, $< 2''$ thereafter). In addition to the X-ray sources in M 67 we observed two ordinary member giants of M 67, S 1288 and S 1402, for comparison. Furthermore one flux standard and three velocity standards were observed. The blue high-resolution spectra of S 1113 were obtained on April 7/8, 1998 with the same telescope through a service observation (seeing $1-2''$). A log of the observations is given in Table 2.

All spectra have been reduced using the Image Reduction and Analysis Facility (IRAF)¹.

¹ IRAF is distributed by the National Optical Astronomy Observatories, which are operated by the Association of Universities for Research in Astronomy, Inc., under cooperative agreement with the National Science Foundation

2.1. Low-resolution spectra

Low-resolution spectra were taken with the ISIS double-beam spectrograph (Carter et al. 1993). The blue arm of ISIS was used with the 300 lines per mm grating and TEK-CCD, resulting in a wavelength coverage of 3831 to 5404 Å and a dispersion of 1.54 Å per pixel at 4000 Å. The red arm, combined with the 316 lines per mm grating and EEV-CCD, covered a wavelength region of 5619 to 7135 Å with a dispersion of 1.40 Å per pixel at 6500 Å. The format of the frames is 1124×200 pixels which includes the under- and overscan regions. For the object exposures the slit width was set to $4''$. Flatfields were made with a Tungsten lamp while CuAr and CuNe lamp exposures were taken for the purpose of wavelength calibration.

For the ISIS-spectra, basic reduction steps have been done within the IRAF CCDRED-package. These steps include removing the bias signal making use of the under- and overscan regions and zero frames, trimming the frames to remove the under- and overscan, and flatfielding to correct for small pixel-to-pixel gain variations. The remaining reduction has been done with IRAF SPECRED-package tasks. With the optimal extraction algorithm (Horne 1986) the two dimensional images are reduced to one dimensional spectra. Next, the spectra are calibrated in wavelength with the arc frames. A dispersion solution is found by fitting third (blue) and fourth (red) order polynomials to the positions on the CCD of the arclamp lines. The fluxes of the spectra are calibrated with the absolute fluxes of HZ 44, tabulated at 50 Å intervals (Massey et al. 1988), and adopting the standard atmospheric extinction curve for La Palma as given by King (1985). The estimated accuracy of the flux calibration is $\sim 10\%$.

2.2. High-resolution spectra

High-resolution echelle spectra were taken with the Utrecht Echelle Spectrograph (UES, Unger et al. 1993). Observations were done with a $\sim 1''$ slitwidth.

For the 1996 observations, the UES was used in combination with a 1024×1024 pixels TEK-CCD, and the 31.6 lines per mm grating (E31), which resulted in a broad wavelength coverage, but small separation of the echelle orders on the CCD. In this setup, the UES resolving power is 49 000 per resolution element (two pixels), corresponding to a dispersion of 3 km s^{-1} per pixel or 0.06 Å per pixel at 6000 Å. The frames were centered on $\lambda_{\text{cen}} = 4250$ Å and $\lambda_{\text{cen}} = 5930$ Å in order to get a blue (3820 to 4920 Å) and red (4890 to 7940 Å) echelle spectrum. The number of orders recorded on the CCD is 34 in the blue and 45 in the red, each covering ~ 45 to 80 Å increasing for longer wavelengths. Towards the red, gaps occur between the wavelength coverage of adjacent orders. Exposures of a quartz lamp were taken to make the flatfield corrections. ThAr exposures served as wavelength calibration frames.

For the 1998 observations of S 1113, a 2048×2048 pixels SITE-CCD was used. Two spectra were taken with the 79.0 lines per mm (E79) grating ($\lambda_{\text{cen}} = 4343 \text{ \AA}$). The difference between the E79 and the E31 gratings is that E79-spectra have a larger separation of the echelle-orders on the detector, which can improve the determination of the sky-background. The spectral resolution of the gratings is the same (the central dispersion in these observations is $\sim 0.04 \text{ \AA}$ per pixel). The specified wavelength-coverage for this combination of grating and detector is 3546 to 6163 \AA but only the central orders were bright enough to extract spectra (3724 to 5998 \AA). Flatfield and ThAr exposures were made for calibration purposes.

The reduction of the UES spectra has been performed using the routines available within the IRAF ECHELLE-package. First, the frames are debiased and the under- and overscan regions removed. After locating the orders on the CCD for both the quartz lamp and the object exposures, we flatfielded the frames. Spectra are extracted with optimal extraction. The small order separation makes sky subtraction difficult; however, our targets are bright, and the resulting error is negligible. In the step of wavelength calibration, the dispersion solution is derived by fitting third and fourth order polynomials leaving rms-residuals of 0.004 \AA (red) and 0.002 \AA (blue, 0.003 \AA for the 1998-spectra). To find absolute fluxes for the Ca II K ($\lambda 3933.67 \text{ \AA}$) & H ($\lambda 3968.47 \text{ \AA}$) emission lines (Sect. 3.1), the fluxes of the relevant blue orders of an object have been calibrated with the calibrated ISIS spectrum of the same object. Continuum normalization of the orders in the red spectra, required for the rotational velocity analysis, is done by fitting third to fifth order polynomials to the wavelength-calibrated spectra.

3. Data analysis

We study two indicators of magnetic activity. The direct indicator is emission in the cores of the Ca II H&K lines. Another indicator is the rotational speed: rapid (differential) rotation and convective motions are thought to generate magnetic fields through a dynamo.

3.1. Determination of Ca II H&K emission fluxes

To estimate the amount of flux emitted in the Ca II H&K line cores, F_{Ca} , we add the fluxes above the H&K absorption profiles as follows. An upper and a lower limit of the level of the absorption pseudo-continuum is estimated by eye and is marked by a straight line. For S 1113 this is illustrated in Fig. 7. We obtain a lower and upper limit of the emitted flux by adding the fluxes in each wavelength-bin above these levels. The value given in Table 3 is the average of these two results, the uncertainty is half their difference. Use of higher order fits (following Fernández-Figueroa et al. 1994) to the absorption profile gives similar results. If an emission line is not clearly visible, we obtain

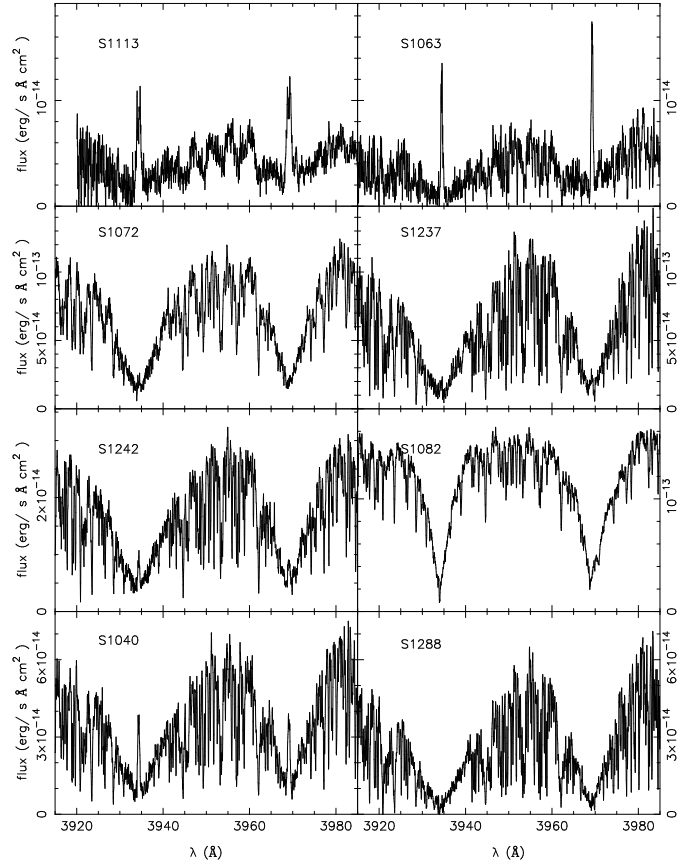


Fig. 2. The Ca II H&K regions in the high-resolution spectra of our targets. In the lower right corner the spectrum of the non-active comparison giant S 1288 is shown.

an upper limit by estimating the minimal detectable emission flux at the H&K line centers within a 1 \AA wide region (typical width of the emission lines).

Six of our sources show Ca II H&K line emission (Fig. 2). The profiles of S 1113 appear to be double-lined, suggesting that we see activity of both stars (Fig. 7). The fluxes given in Table 3 are the total fluxes, i.e. no attempt was made to deblend the emission lines. No emission is visible in the spectrum of S 1082.

3.2. Determination of projected rotational velocities

3.2.1. Crosscorrelation

In order to derive the projected rotational velocity $v \sin i$ of our targets, we apply the crosscorrelation technique (e.g. Tonry & Davis 1979). This method computes the correlation between the object spectrum and an appropriately chosen template spectrum as function of relative shift. The position of the maximum of the crosscorrelation function (CCF) provides the value of the radial-velocity difference between object and template. The width of the peak is indicative for the width of the spectral lines and

Table 3. Fluxes of emission cores in Ca II H&K lines and projected rotational velocities derived from our high-resolution spectra. The velocities were determined from crosscorrelation with the spectrum of HD 136202 (F8III-IV, ESA 1997) for S 1040, S 1072, S 1082 and S 1242; and with the spectrum of HD 171232 (G8III, ESA 1997) for the other stars. Both HD stars have line widths $\tau = 1.8 \pm 0.1 \text{ km s}^{-1}$. For S 1113 we list both components; the primary contributes $\sim 82\%$ of the light and has broader lines.

| ID | $\log F_{\text{CaK}}$ ($\text{erg cm}^{-2} \text{ s}^{-1}$) | $\log F_{\text{CaH}}$ ($\text{erg cm}^{-2} \text{ s}^{-1}$) | $v \sin i$ (km s^{-1}) |
|--------|--|--|--------------------------------------|
| S 1040 | $16(4) \times 10^{-15}$ | $17(5) \times 10^{-15}$ | 3.0(1.0) |
| S 1063 | $6(1) \times 10^{-15}$ | $7(1) \times 10^{-15}$ | 3.9(0.8) |
| S 1072 | $3(2) \times 10^{-15}$ | $< 13 \times 10^{-15}$ | 8.1(1.1) |
| S 1082 | $< 11 \times 10^{-15}$ | $< 24 \times 10^{-15}$ | 5.1(0.7) |
| S 1113 | $9(2) \times 10^{-15}$ | $10(3) \times 10^{-15}$ | 45(6) 12(1) |
| S 1237 | $4(2) \times 10^{-15}$ | $8(5) \times 10^{-15}$ | < 1.8 |
| S 1242 | $2.2(0.5) \times 10^{-15}$ | $2(1) \times 10^{-15}$ | $< 2.6(1.0)$ |

can therefore be used as a measure of the rotational velocity of the stars.

For rotational velocities not too large the line profiles may be approximated with Gaussians, allowing analytical treatment of the crosscorrelation method. Assuming that the binary spectrum is a shifted, scaled and broadened version of the template spectrum, the broadening can be related to the width of the CCF peak as follows (Gunn et al. 1996). With τ the dispersion in the template's and β the dispersion in the target's spectral lines, μ the dispersion of the CCF peak and σ the dispersion of the gaussian that describes the broadening of the object's spectrum with respect to the template, one can write:

$$\mu^2 = \tau^2 + \beta^2 = 2\tau^2 + \sigma^2 \quad (1)$$

Eq. 1 applies to both components in the binary spectrum and their corresponding CCF peaks.

The crosscorrelations are performed with the IRAF task FXCOR that uses Fourier transforms of the spectra to compute the CCF. Before performing the crosscorrelation, the continuum is subtracted from the normalized spectra. Filtering in the Fourier domain is applied to avoid undesirable contributions originating from noise or intrinsically broad lines (see Wyatt 1985).

The templates are chosen from the radial-velocity standards such that their spectral types resemble those of the targets. The value of τ for these stars is determined for each order separately by autocorrelation of the template spectrum adopting the same filter used for the crosscorrelations. In this case σ is zero and therefore τ is found directly from the width of the CCF peak: $\tau^2 = \mu^2/2$.

The template spectra are correlated with our target stars order by order, where we limit ourselves to orders in

the red spectra that do not suffer from strong telluric lines. Most CCF peaks can be fitted well with a gaussian. As the final value for $v \sin i$ we give the broadening σ averaged over the different orders, and for the uncertainty we take the rms of the spread around the average of σ (Table 3). Equating $v \sin i$ to σ implicitly assumes that τ is the width of the lines not related to rotation. An upper limit to $v \sin i$ is found from the other extreme in which we assume that the total width of the spectral line β follows from rotation. This creates uncertainties of the order of σ for S 1242. In the case of S 1237 we find that $\beta < \tau$ ($\sigma < 0$), i.e. the lines in S 1237 are narrower than in the template. For these two stars, we give an upper limit of $v \sin i < \beta$ in Table 3.

S1113 is the only binary observed whose CCF shows two peaks. The CCF peaks of both stars overlap in the 1998 observation. Therefore we do not use these spectra in the following analysis. For the 1996 spectra, the CCF shows two peaks, one of which is broad indicating the presence of a fast rotating star. Both peaks are clearly separated with a center-to-center velocity separation of $\sim 110 \text{ km s}^{-1}$. The lines in the spectrum are smeared out and less pronounced, resulting in a noisy CCF. To improve this, we combine four sequential orders before crosscorrelating (being constrained by the maximum number of points FXCOR can handle). From eq. 17 in Gunn et al. we derive the relative light contribution of both components to the spectrum from the height and dispersion of the crosscorrelation peaks, assuming that the binary stars have the same spectrum as the template ($\alpha = 1$ in eq. 17). According to this the rapidly rotating star contributes $\sim 82\%$ of the light. Note that luminosity ratios derived from crosscorrelations are uncertain and should be confirmed photometrically.

3.2.2. Fourier-Bessel transformation

The line profile of the fast rotating star in S 1113 is not compatible anymore with a Gaussian, therefore we adopt another method to determine its $v \sin i$, described in Pitters et al. (1996). This method uses the property that the Fourier-Bessel transform of a spectral line that is purely rotationally broadened has a maximum at the position of the projected rotational velocity. In practice, this position is a function of the limits over which the Fourier transform is performed. The local maxima of this velocity-versus-cutoff-frequency (vcf) function approach $v \sin i$ within half a percent, the result growing more accurate for maxima at higher frequencies. This error is negligible when compared to errors arising from noise, other line broadening mechanisms, etc. (see Pitters et al. 1996). In our determination of $v \sin i$ of the primary of S 1113, we have used the first local maximum in the vcf-plot of the transformation of four isolated Fe I lines at $\lambda\lambda$ 6265.14, 6400.15, 6408.03 and 6411.54 Å. The $v \sin i$ in Table 3 is an average of the resulting values; the $v \sin i$ of the secondary is found from crosscorrelation.

The application of the Fourier-Bessel transformation method is limited on the low velocity side by the spectral resolution: the Fourier transform cannot be performed beyond the Nyquist frequency which for slow rotators lies at a frequency that is lower than the cutoff-frequency at which the first maximum occurs in the vcf-plot. For our spectra this means that the method cannot be used for $v \sin i < 5.2 \text{ km s}^{-1}$. Indeed, for every star for which the crosscorrelation method gives a $v \sin i$ smaller than this value, the vcf-plot does not reach the first local maximum, except for S 1082 for which we find $v \sin i = 9.5(1.6)$. For S 1072, the Fourier-Bessel transform gives a $v \sin i$ of $12.7(1.0) \text{ km s}^{-1}$. Spectral lines were selected from those used in Groot et al. (1996) and from the additional lines used for S 1113.

4. Results

The results of our search for emission cores in the Ca II H&K lines are displayed in Fig. 2 and in Table 3. The emission lines are strong in S 1063, S 1113 and S 1040; and still detectable in S 1242 which indicates chromospheric activity in these stars. In S 1072 and S 1237 the emission cores are marginal, and on S 1082 we can only determine an upper limit.

The (projected) rotational velocities of all of our stars are relatively small $v \sin i < 10 \text{ km s}^{-1}$, with the exception of S 1113.

In Sect. 4.1 we investigate whether the relations between X-ray emission, strength of the emission cores in the Ca II H&K lines, and the rotational velocities of the unusual X-ray emitters in M 67 are similar to the relations found for well-known magnetically active stars, the RS CVn binaries. In Sect. 4.2 we briefly discuss the behaviour of the H α line and spectral lines other than Ca II H&K that are indicators of chromospheric activity. Individual systems are discussed in Sect. 4.3.

4.1. Comparison with RS CVn binaries

To investigate whether the X-rays of the M 67 stars studied in this paper are related to magnetic activity, we compare their optical activity indicators and X-ray fluxes with those of a sample of RS CVn binaries. In particular, we select RS CVn binaries for which fluxes of the emission cores in the Ca II H&K lines have been determined from high-resolution spectra by Fernández-Figueroa et al. (1994). To obtain X-ray countrates for these binaries, we searched the ROSAT data archive for PSPC observations of them. We then analyzed all these observations, and determined the countrates, in the same bandpass as used in the analysis of M 67, using the standard procedure described in Zimmermann et al. (1994). All pointings that we have analyzed actually led to a positive detection of the RS CVn system: even when not the target of the observation, the RS CVn

system is usually the brightest object in the field of view. The results of our analysis are listed in Table 4.

To compare systems at different distances, we multiply the ROSAT countrate and the flux of the emission cores for each system with the square of the distance listed in Table 4; for M 67 we adopt a distance of 850 pc (Twarog & Anthony-Twarog 1989). No corrections are made for interstellar absorption. The choice of the 0.4–2.4 keV bandpass minimizes the effects of interstellar absorption, which are severe at energies $< 0.4 \text{ keV}$. As it is unknown which component of the binary emits the X-rays, we plot the total X-ray and Ca II fluxes, adding the contributions of both components where these are given separately by Fernández-Figueroa et al. (1994).

The resulting 'absolute' countrates and fluxes are shown in Fig. 3. The M 67 systems with Ca II H&K emission clearly visible in Fig. 2, viz. S 1063, S 1113, S 1040 and S 1242 lie on the relation between X-ray and Ca II H&K emission defined by the RS CVn systems, in agreement with the hypothesis that the X-ray flux of these objects is related to the magnetic activity. It is also seen that the upper limits or marginally detected emission cores in S 1082, S 1072 and S 1237 are high enough that we cannot exclude the hypothesis that the X-ray emission in these systems is related to magnetic activity.

The rotational velocity is another indicator of magnetic activity. We investigate the relation between rotational velocity and Ca emission by selecting those stars from the sample of Fernández-Figueroa for which a value of $v \sin i$ is given in the Catalogue of Chromospherically Active Binary Stars (Strassmeier et al. 1993). In Fig. 4 the Ca II H&K emission of these stars is compared with their $v \sin i$. In this figure we do discriminate between the separate contributions of both stars to F_{Ca} , with the exception of S 1113 for which we combine the total flux F_{Ca} with the $v \sin i$ of the primary. The M 67 stars are found within the range occupied by chromospherically active stars. We note that the correlation between the observed H&K flux and $v \sin i$ is not tight. In particular, high and low Ca II H&K emission flux is found at low values of $v \sin i$. Some of the scatter may be due to the use of $v \sin i$ instead of the stellar rotation period.

Parameters depending on the spectral type (e.g. properties of the convective region) have been used to reduce the scatter in the activity-rotation relation; whereas this is successful for main-sequence stars with $0.5 \lesssim B - V \lesssim 0.8$, it fails for other main-sequence stars and for giants (see discussion in Stępień 1994). For example, the three giants 33 Psc (K0 III), 12 Cam (K0 III) and DR Dra (K0-2 III) have $v \sin i$ values of 10, 10 and 8 km s^{-1} , respectively, but differ in $\log d^2 F_{\text{Ca}}$ by three orders of magnitude (see Fig. 4).

Table 4. ROSAT PSPC countrates for RS CVn binaries, from our analysis of archival data. For each source we list the distance, adopted from the Hipparcos catalogue (ESA 1997), the Julian date (-2440000) of the beginning of the ROSAT exposure, the effective exposure time, the countrate in channels 41–240 (i.e. roughly in the 0.4–2.4 keV band), and the offset of the star to the ROSAT pointing direction. Where applicable we also refer to earlier publication of the ROSAT observation: ^aSingh et al. (1996a), ^bWelty & Ramsey (1995), ^cWhite et al. (1994), ^dYi et al. (1997), ^eSingh et al. (1996b), ^fBauer & Bregman (1996), ^gOrtolani et al. (1997).

| name | d (pc) | JD | t_{exp} (s) | ctrate (s^{-1}) | Δ ($'$) |
|-----------------------------------|----------------|----------|-------------------------|-------------------------------|---------------------|
| LUMINOSITY CLASS V (GROUP 1) | | | | | |
| IL Com | 107 ± 12 | 8420.575 | 16156 | 0.322(5) | 36 |
| | | 8775.123 | 8345 | 0.126(5) | 36 |
| TZ CrB | 21.7 ± 0.5 | 8864.531 | 4267 | 6.072(15) | 0 |
| | | 9003.872 | 5776 | 6.228(11) | 0 |
| | | 8864.595 | 3651 | 6.84(2) | 24 |
| | | 9004.871 | 3151 | 5.41(2) | 24 |
| V772 Her | 37.7 ± 1.9 | 9049.117 | 14531 | 1.206(4) | 0 |
| BY Dra | 16.4 ± 0.2 | 9247.809 | 9895 | 1.009(7) | 0 |
| V775 Her ^a | 21.4 ± 0.5 | 9085.714 | 2140 | 1.10(2) | 0 |
| ER Vul | 49.9 ± 2.1 | 9148.099 | 1209 | 1.23(3) | 0 |
| KZ And | 25.3 ± 4.9 | 8604.712 | 5249 | 0.888(16) | 36 |
| LUMINOSITY CLASS IV (GROUP 2) | | | | | |
| V711 Tau | 29.0 ± 7 | 8648.446 | 3098 | 6.29(2) | 0 |
| UX Com | 168 ± 51 | 8426.486 | 21428 | 0.146(3) | 33 |
| RS CVn | 108 ± 12 | 8810.279 | 2526 | 0.336(17) | 44 |
| | | 8991.040 | 6214 | 0.372(11) | 44 |
| | | 8796.874 | 5076 | 0.305(12) | 51 |
| | | 8966.506 | 2904 | 0.366(18) | 51 |
| HR 5110 | 44.5 ± 1.2 | 8431.422 | 71803 | 2.3152(14) | 44 |
| | | 9158.435 | 37658 | 2.403(3) | 44 |
| SS Boo ^b | 202 ± 57 | 9030.359 | 10327 | 0.059(2) | 0 |
| RT Lac ^b | 193 ± 39 | 8789.392 | 8668 | 0.198(5) | 0 |
| AR Lac ^c | 42.0 ± 1.0 | 8620.767 | 13460 | 1.717(4) | 0 |
| | | 9136.873 | 4892 | 2.902(13) | 0 |
| LUMINOSITY CLASS III/II (GROUP 3) | | | | | |
| 12 Cam | 192 ± 34 | 8322.477 | 3516 | 0.574(13) | 3 |
| σ Gem ^d | 37.5 ± 1.1 | 8346.927 | 4745 | 5.269(14) | 0 |
| | | 8904.569 | 1438 | 3.43(4) | 0 |
| | | 8735.159 | 7940 | 4.753(8) | 0 |
| DK Dra | 138 ± 10 | 9272.484 | 4156 | 1.32(2) | 41 |
| ϵ UMi | 106 ± 7.6 | 8328.919 | 14690 | 0.624(6) | 40 |
| DR Dra ^e | 103 ± 8.5 | 8863.981 | 10576 | 1.554(8) | 31 |
| HR 7428 ^e | 323 ± 53 | 9088.631 | 24889 | 0.112(2) | 0 |
| IM Peg | 96.8 ± 7.1 | 8589.200 | 6335 | 1.692(15) | 44 |
| | | 8769.630 | 8150 | 1.422(12) | 44 |
| | | 8973.263 | 22143 | 1.909(4) | 44 |
| λ And ^{f,g} | 25.8 ± 0.5 | 8448.155 | 31165 | 4.077(2) | 0 |

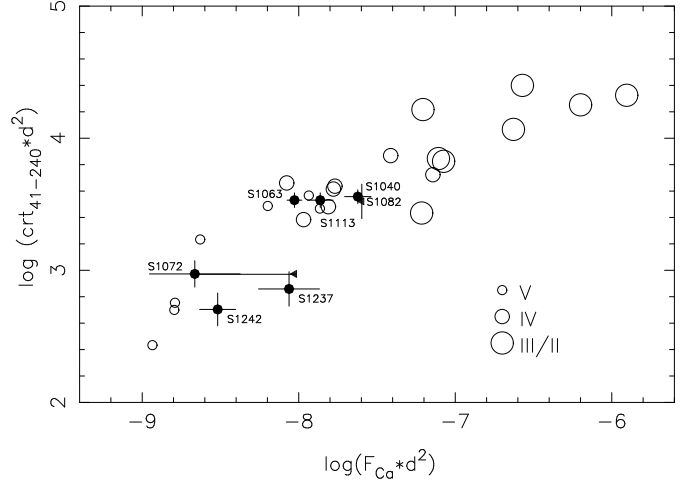


Fig. 3. PSPC countrates in channels 41–240 versus observed Ca II H&K emission flux F_{Ca} (in $\text{erg s}^{-1}\text{cm}^{-2}$). Both are multiplied with the square of the distance (in pc). Open circles are chromospherically active binaries from the sample of Fernández-Figueroa (1994). Their size indicates the luminosity class of the active component. When more than one PSPC observation is available, the countrate of the longest exposure is plotted. Filled symbols are the M 67-sources. Triangles indicate upper limits.

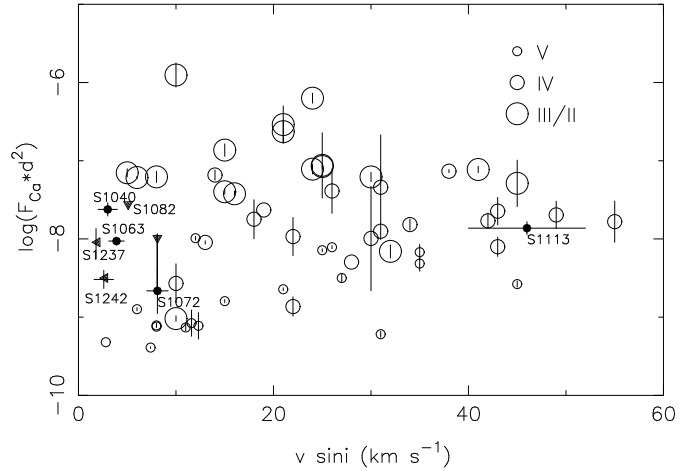


Fig. 4. Observed Ca II H&K emission flux F_{Ca} versus $v \sin i$. Open circles show the comparison sample of chromospherically active binaries up to 60 km s^{-1} (Strassmeier et al. 1993 and Fernández-Figueroa 1994). Their size indicates the luminosity class of the active star. Vertical bars indicate $1\text{-}\sigma$ errors due to uncertainty in the distance, for systems with a Hipparcos parallax. M 67 sources are plotted as filled symbols.

4.2. Activity indicators

The H α lines ($\lambda 6562.76 \text{ \AA}$) of only two stars, S 1063 and S 1113, show clear evidence of emission, as shown in Fig. 6. This is described in more detail in their individual subsection in Sect. 4.3. For the other M 67 stars, we have used the

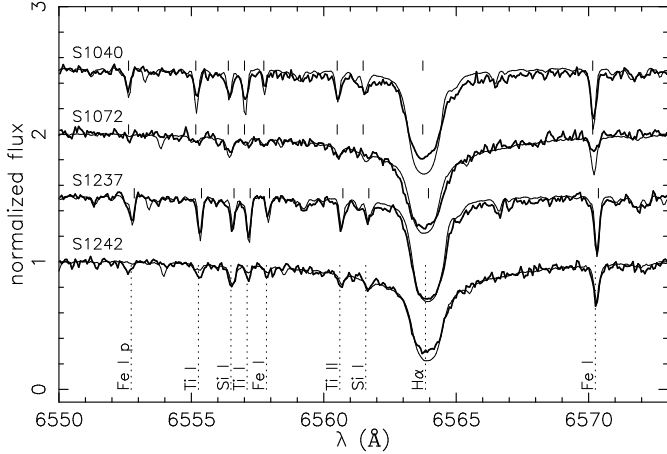


Fig. 5. $H\alpha$ profiles of S 1040, S 1072, S 1237 and S 1242. Library UES-spectra (Montes & Martín 1998) are plotted with a thinner line. The comparison star is a K0III giant (HD 48432) for S 1040 and S 1237, and a G0IV–V subgiant (HD 160269) for the other stars. Position of $H\alpha$ and other lines are indicated with vertical lines.

few (sub)giants in the library of UES-spectra of Montes & Martín (1998) to investigate the behaviour of $H\alpha$. We have chosen library spectra of stars that match the spectra of the M 67 stars as closely as possible (see Fig. 5). S 1072 and S 1237 show no evidence for filling in of the $H\alpha$ profile compared to a G0IV–V and a K0III star, respectively. In S 1040 $H\alpha$ seems slightly filled in compared to a G8IV and a K0III star. This is also the case for S 1242 compared to a G0IV–V star, but we note that no classification for this star is found in literature. For S 1082, no matching spectrum is available in this wavelength region.

Filling in of the lines in the Mg I b triplet ($\lambda\lambda$ 5167.33, 5172.70 and 5183.62 Å) and in the Na I D doublet ($\lambda\lambda$ 5889.95 and 5895.92 Å) is visible in some active stars. The presence of a He I D₃ (λ 5876.56) absorption or emission feature can also indicate activity (see discussion in Montes & Martín (1998) and references therein). However, in none of the M 67 stars we see filled in Mg I b and Na I D lines. Neither do we see a clear He I D₃ feature. For S 1082 (Mg I b and Na I D) and S 1113 (Mg I b, Na I D and He I D₃) we find no suitable library stars for these features.

4.3. Individual systems

4.3.1. S 1063 and S 1113

The two stars below the subgiant branch, S 1063 and S 1113, both show relatively strong Ca II H&K emission, and are the only two stars in our sample showing $H\alpha$ in emission, shown in Fig. 6. We use the orbital solutions for both objects to try and identify the star responsible for these emission lines. The velocities of both components in S 1113, and of one component in S 1063 are indicated in Fig. 6.

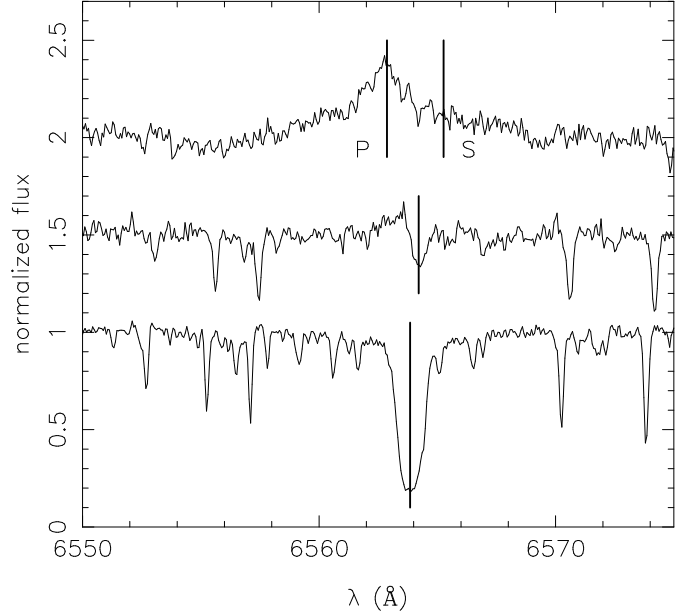


Fig. 6. $H\alpha$ in S 1113 (top), S 1063 (middle) and comparison giant S 1288. The intensity is normalized to the continuum level; the upper two spectra are displaced vertically by 0.5 and 1 unit. The line marks the radial velocity shift of the stars as determined by the crosscorrelation; for S 1113 the primary (P) and secondary (S) star are separately indicated.

The $H\alpha$ line profile of S 1063 is asymmetric, showing emission which is blue-shifted with respect to the absorption. The location of the absorption line is compatible with the velocity of the primary, which dominates the flux; the emission is probably due to the secondary. Remarkably, the Ca II H&K emission peak is at the velocity of the primary. This suggests that the $H\alpha$ emission is not chromospheric in nature. The $H\alpha$ emission of S 1063 does not show the double peak that is known to indicate accretion disk emission (Horne & Marsh, 1986).

In S 1113 the $H\alpha$ emission profile is symmetric and broad, with full width at continuum level of 15 Å. The emission peak is centered on the more massive star, which contributes 82% of the total flux (Table 3). This suggests that the $H\alpha$ emission is due to the primary. The Ca II H&K emission shows marginal evidence for a double peak, suggesting that both stars contribute to the chromospheric emission. In Fig. 7 we indicate the expected position of the H&K lines for both stars. For the phase observed, their peaks overlap in the crosscorrelation function. In the figure we use the velocities resulting from fitting the order that gives the ‘cleanest’ crosscorrelation.

4.3.2. S 1072 and S 1237

The Ca II H&K emission in the wide binaries S 1072 and S 1237 is only marginally significant. The level of their X-

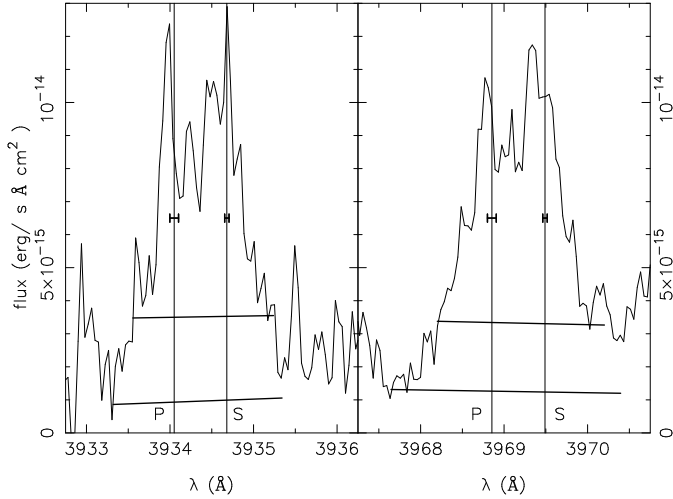


Fig. 7. Ca II H&K emission cores in S 1113. The vertical lines mark the shifted position of the lines for the primary (P) and secondary (S) as derived from the crosscorrelation with the radial velocity standard HD 132737 (K0III, ESA 1997). Errors are also indicated. The long horizontal lines indicate the upper and lower limit chosen to determine the emitted Ca II H&K flux (see Sect. 3.1).

ray and Ca II emission is more appropriate for active main-sequence stars (Fig. 3). One might speculate that it is due to the invisible companion of the giant detected in the crosscorrelation; even if this were the case, we would not understand why this companion would be chromospherically active. We conclude that we do not understand why these two stars are X-ray sources. We find no indication for a faint secondary in the crosscorrelation profile of S 1237; at the time of observation, the spectra of two equally massive stars as suggested by Janes & Smith (1984) would be separated by 4 to 7 km s⁻¹ (derived from the ephemeris in Mathieu et al. 1990). Since the secondary is 1.6 magnitude fainter in V than the primary, we think that this small separation is compatible with finding a single peak in the crosscorrelation.

4.3.3. S 1242

S 1242 is chromospherically active, as shown by its Ca II H&K emission. We suggest that this activity, which also explains the X-rays, is due to rapid rotation induced by tidal interaction at periastron, which tries to bring the subgiant into corotation with the orbit at periastron. If we assume that the observed period of photometric variability is the rotation period we derive an inclination of $\sim 9^\circ$ using our maximum value of $v \sin i$ and the estimated radius. This would be in agreement with a companion at the high end of the range 0.14–0.94 M_\odot allowed by the mass function (Mathieu et al. 1990).

4.3.4. S 1040

Our detection of clear chromospheric emission indicates that the X-ray emission of S 1040 is due to the giant. The white dwarf has a low temperature, and is unlikely to contribute to the X-ray flux. We find a rather slow rotational velocity for the giant, 3 km s⁻¹. Gilliland et al. (1991) detected a periodicity of 7.97 days in the visual flux (B and V bandpasses) of S 1040, with an amplitude of 0.012 mag. If this is the rotation period of the giant, the radius of 5.1 R_\odot (Landsman et al. 1997) implies an equatorial rotation velocity of $v = 32$ km s⁻¹. This is compatible with the velocity measured with our crosscorrelation, $v \sin i$, for an inclination $i \lesssim 5.3^\circ$. This inclination has an a priori probability less than 0.5%; and it implies an unacceptably high mass for the white dwarf, from the measured mass function $f(m) = 0.00268$. We conclude that the 8 days period cannot be the rotation period of the giant. It is doubtful that the white dwarf can be responsible, as its contribution to the B and V flux is small.

4.3.5. S 1082

The H α absorption profile of the blue straggler S 1082 is variable. If we consider the most symmetric spectrum profile, that of 00:01 UT, as the unperturbed profile of the primary, we find that the changes are due to extra emission. This is illustrated in Fig. 8. We suggest that this variation is due to the subluminescent companion, possibly to a wind of that star. We have also investigated the presence of a broad shallow depression underlying the Na I D lines (near $\lambda 5895$ Å) and the O I triplet (near $\lambda 7775$ Å) as found by Mathys (1991). We find that this broad component is variable, as illustrated in Fig. 9. Mathys (1991) suggests that the broad component originates in the subluminescent companion. This companion outshines the primary by a factor six at $\lambda 1500$ Å and thus is presumably hot (Landsman et al. 1998). We note that the star cannot be too hot or it would not show neutral lines.

5. Discussion and conclusions

In this paper we have tried to find an explanation for the X-ray emission of seven sources in M 67.

For S 1242 and S 1040 we have concluded from the Ca II H&K emission cores that magnetic activity is responsible for the X-rays. This is supported by filling in of H α (see e.g. Montes et al. 1997; Eker et al. 1995). In S 1242, activity is likely to be triggered by interaction at periastron in the eccentric orbit. This is also reflected in the period of photometric variability. For S 1040, the reason for activity is less clear. The explanation could involve mass transfer from the precursor of the white dwarf to the giant and the latter's subsequent expansion during the giant phase. As was already noted by Landsman et al. (1997), a similar system is AY Cet, a binary of a white dwarf of

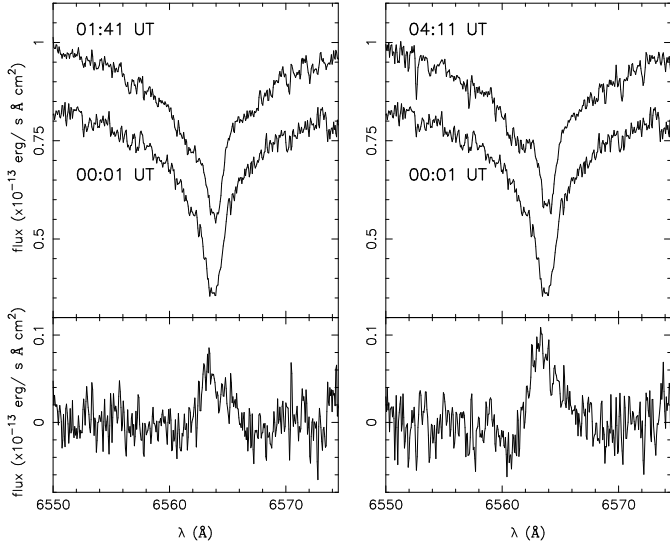


Fig. 8. $H\alpha$ profile for the three exposures of S 1082. The spectra are labelled according to the UT at start of the exposure. For clarity, the lower spectrum is offset with $-0.2 \times 10^{-13} \text{ erg s}^{-1} \text{ \AA}^{-1} \text{ cm}^{-2}$ in both figures. The lower panels show the difference between the first and second (left) and the first and the third exposure.

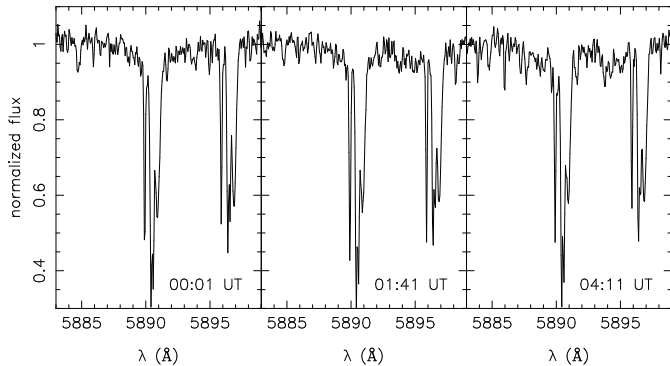


Fig. 9. Na I D lines in S 1082. Shown from left to right are the three spectra labelled according to the UT at start of the exposure. Variability is most clearly seen left of the Na λ 5895.92 line.

$T_{\text{eff}} = 18000 \text{ K}$ (Simon et al. 1985) and a G5III giant in an 56.8 days circular orbit. The $v \sin i$ of that giant is also low, 4 km s^{-1} , and the long photometric period of 77.2 days implies asynchronous rotation (Strassmeier et al. 1993). The X-ray luminosity for AY Cet is $1.5 \times 10^{31} \text{ erg s}^{-1}$ in the 0.2–4 keV band as measured with Einstein by Walter & Bowyer (1981), somewhat higher than the luminosity of S 1040. (With the coronal model discussed by Belloni et al. (1998), the countrate for S 1040 corresponds to $5.6 \times 10^{30} \text{ erg s}^{-1}$ in the 0.2–4 keV band.) Walter & Bowyer attribute the X-rays to coronal activity of the giant.

The Ca II H&K emission cores in S 1063 and S 1113 are very strong. In S 1113 we might even see emission of both

stars. Due to the shape of the $H\alpha$ emission we cannot conclude with certainty that the X-rays arise in an active corona and not in a disk or stream. The wings in the emission peak of S 1113 are very broad. However, Montes et al. (1997) have demonstrated that the excess emission in the $H\alpha$ lines of the more active binaries is sometimes a composite of a narrow and broad component, the latter having a full width at half maximum of up to 470 km s^{-1} . They ascribe this broad component to microflaring accompanied by large scale motions. We note the similarity between S 1113 and V711 Tau, a well known extremely active binary of a G5IV ($v \sin i = 13 \text{ km s}^{-1}$) and K1IV ($v \sin i = 38 \text{ km s}^{-1}$) star in a 2.84 days circular orbit and a mass ratio 0.79 (Strassmeier et al. 1993); the mass ratio of S 1113 is 0.70 (Mathieu et al. 1998, in preparation). From the countrate of V711 Tau in Table 4 we find $L_x = 6.8 \times 10^{30} \text{ erg s}^{-1}$ in the 0.1–2.4 keV band using the same model as in Belloni et al. (1998) with $N_H = 0$, which is comparable to the luminosity of S 1113 in the same band $L_x = 7.3 \times 10^{30} \text{ erg s}^{-1}$ (Belloni et al. 1998). The $H\alpha$ emission of S 1063 is more difficult to explain. As this system is not double-lined, $H\alpha$ emission by the (invisible) secondary star would have to be strong to rise above the continuum of the primary.

In the binaries S 1072 and S 1237 we see no $H\alpha$ emission while the level of Ca II H&K emission is low in comparison with active stars of the same luminosity class. We have no explanation for this. For S 1072, an option is a wrong identification of the X-ray source with an optical counterpart. Belloni et al. (1998) give a probability of 43% that one or two of their twelve identifications of an X-ray source with a binary in M 67 is due to chance.

No Ca II H&K emission is seen in the spectrum of the blue straggler S 1082. Possibly, the X-ray emission has to do with the hot, subluminous secondary that could also cause the photometric variability and whose signature we might have seen in the $H\alpha$ line.

Acknowledgements. The authors wish to thank G. Geertsema for her help during our observations, P. Groot for providing his program to compute projected rotational velocities with the Fourier-Bessel transformation method and M. van Kerkwijk for comments on the manuscript. MvdB is supported by the Netherlands Organization for Scientific Research (NWO).

References

- Allen, L. E., Strom, K. M. 1995, AJ, 109, 1379
- Bauer, F., Bregman, J. N. 1996, ApJ, 457, 382
- Belloni, T., Verbunt, F., Mathieu, R. D. 1998, A&A, 339, 431
- Belloni, T., Verbunt, F., Schmitt, J. H. M. M. 1993, A&A, 269, 175
- Carter, D., Benn, C. R., Rutten, R. G. M., Breare, J. M., Rudd, P. J., King, D. L., Clegg, R. E. S., Dhillon, V. S., Arribas, S., Rasilla, J.-L., Garcia, A., Jenkins, C. R., Charles, P. A. 1993, ISIS Users' Manual, <http://www.ing.iac.es>
- Eker, Z., Hall, D. S., Anderson, C. M. 1995, ApJS, 96, 581

- ESA 1997, The Hipparcos and Tycho Catalogues, ESA SP 1200
- Fernández-Figueroa, M. J., Montes, D., Castro, E. D., Cornide, M. 1994, *ApJS*, 90, 433
- Gilliland, R. L., Brown, T. M., Duncan, D. K., Suntzeff, N. B., Lockwood, G. W., Thompson, D. T., Schild, R. E., Jeffrey, W. A., Penrose, B. E. 1991, *AJ*, 101, 541
- Goranskij, V. P., Kusakin, A. V., Mironov, A. V., Moshkaljov, V. G., Pastukhova, E. N. 1992, *Astron. Astrophys. Trans.*, 2, 201
- Groot, P. J., Pitters, A. J. M., van Paradijs, J. 1996, *A&AS*, 118, 545
- Gunn, A. G., Hall, J. C., Lockwood, G. W., Doyle, J. G. 1996, *A&A*, 305, 146
- Hobbs, L. M., Mathieu, R. D. 1991, *PASP*, 103, 431
- Horne, K. 1986, *PASP*, 98, 609
- Horne, K., Marsh, T. R. 1986, *MNRAS*, 218, 761
- Janes, K. A., Smith, G. H. 1984, *AJ*, 89, 487
- Kaluzny, J., Radczynska, J. 1991, *IBVS* 3586
- King, D. L. 1985, *ING Technical Note*, 31
- Kippenhahn, R., Weigert, A. 1967, *Zeitschrift für Astrophysik*, 65, 251
- Kurochkin, N. E. 1960, *Astron. Circular USSR*, 212, 9
- Landsman, W., Aparicio, J., Bergeron, P., Di Stefano, R., Stecher, T. P. 1997, *ApJ*, 481, L93
- Landsman, W., Bohlin, R. C., Neff, S. G., O'Connell, R. W., Roberts, M. S., Smith, A. M., Stecher, T. P. 1998, *AJ*, 116, 789
- Latham, D. W., Mathieu, R. D., Milone, A. A. E., Davis, R. J. 1992, in A. Duquennoy, M. Mayor (eds.), *Binaries as tracers of stellar formation*, Cambridge University Press, Cambridge, 132
- Massey, P., Strobel, K., Barnes, J. V., Anderson, E. 1988, *ApJ*, 328, 315
- Mathieu, R. D., Latham, D. W. 1986, *AJ*, 92, 1364
- Mathieu, R. D., Latham, D. W., Griffin, R. F. 1990, *AJ*, 100, 1859
- Mathieu, R. D., Latham, D. W., Griffin, R. F., Gunn, J. E. 1986, *AJ*, 92, 1100
- Mathys, G. 1991, *A&A*, 245, 467
- Montes, D., Fernández-Figueroa, M. J., De Castro, E., Sanz-Forcada, J. 1997, *A&AS*, 125, 263
- Montes, D., Martín, E. L. 1998, *A&AS*, 128, 485
- Montgomery, K. A., Marshall, L. A., Janes, K. A. 1993, *AJ*, 106, 181
- 11
- Nissen, P. E., Twarog, B. A., Crawford, D. L. 1987, *AJ*, 93, 634
- Ortolani, A., Maggio, A., Pallavicini, R., Sciortino, S., Drake, J. J., ADrake, S. 1997, *A&A*, 325, 664
- Pasquini, L., Belloni, T. 1998, *A&A*, 336, 902
- Pitters, A. J. M., Groot, P. J., van Paradijs, J. 1996, *A&AS*, 118, 529
- Pritchett, C. J., Glaspey, J. W. 1991, *ApJ*, 373, 105
- Rajamohan, R., Bhattacharyya, J. C., Subramanian, V., Kuppuswamy, K. 1988, *Bull. Astr. Soc. India*, 16, 139
- Sanders, W. L. 1977, *A&AS*, 27, 89
- Simoda, M. 1991, *IBVS* 3675
- Simon, T., Fekel, F. C., Gibson, D. M. 1985, *ApJ*, 295, 153
- Singh, K. P., Drake, S. A., White, N. E. 1996a, *AJ*, 111, 2415
- Singh, K. P., Drake, S. A., White, N. E. 1996b, *AJ*, 112, 221
- Stępień 1994, *A&A*, 292, 191
- Strassmeier, K. G., Hall, D. S., Fekel, F. C., Scheck, M. 1993, *A&AS*, 100, 173
- Tonry, J., Davis, M. 1979, *AJ*, 84, 1511
- Twarog, B. A., Anthony-Twarog, B. J. 1989, *AJ*, 97, 759
- Unger, S., Walton, N., Pettini, M., Tinbergen, J. 1993, *UES Users' Manual*, <http://www.ing.iac.es/>
- Verbunt, F., Phinney, E. S. 1995, *A&A*, 296, 709
- Walter, F. M., Bowyer, S. 1981, *ApJ*, 245, 671
- Welty, A. D., Ramsey, L. W. 1995, *AJ*, 109, 2187
- White, N. E., Arnaud, K., Day, C. S. R., Ebisawa, K., Gotthelf, E. V., Mukai, K., Soong, Y., Yaqoob, T., Antunes, A. 1994, *PASJ*, 46, L97
- Wyatt, W. F. 1985, in A. G. Davis Philip, D. W. Latham (eds.), *Stellar radial velocities*, Vol. 88 of *IAU Coll.*, L. Davis Press, Inc., Schenectady, N.Y., 123
- Yi, Z., Elgarøy, Ø., Engvold, O., Westergaard, N. J. 1997, *A&A*, 318, 791
- Zhilinskii, E. G., Frolov, V. N. 1994, *Astronomy Letters*, 20, 80
- Zimmermann, H., Becker, W., Belloni, T., Döbereiner, S., Izzo, C., Kahabka, P., Schwentker, O. 1994, *EXSAS User's Guide: Extended scientific analysis system to evaluate data from the astronomical X-ray satellite ROSAT*, Technical Report 257, MPE